Proc. Natl. Acad. Sci. USA
Vol. 80, pp. 3769–3773, June 1983
Immunology

Neutron scattering studies of the isolated $C1r_2C1s_2$ subunit of first component of human complement in solution

(glycoproteins/ultracentrifugation)

J. BOYD*, D. R. BURTON†, S. J. PERKINS‡§, C. L. VILLIERS¶, R. A. DWEK*, AND G. J. ARLAUD¶

*Department of Biochemistry, South Parks Road, Oxford OX1 3QR, United Kingdom; †Department of Biochemistry, University of Sheffield, Sheffield S10 2TN, United Kingdom; ‡European Molecular Biology Laboratory, Grenoble Outstation, c/o I.L.L., 156X, 38042 Grenoble Cédex, France; ¶Equipe de Recherche 'Immunochimie—Système complémentaire' de D.R.F.-G et de l'U.S.M.-G, associée au C.N.R.S. (E.R.A. No. 695) et à l'I.N.S.E.R.M. (U. No. 238), Laboratoire de Biologie Moléculaire et Cellulaire, Centre d'Etudes Nucléaires de Grenoble, 85X, 38041 Grenoble Cédex, France

Communicated by R. R. Porter, February 22, 1983

ABSTRACT **The subunit complex $C1r_2C1s_2$ of the first component of complement was investigated by small-angle neutron scattering in both the activated and unactivated forms. From these experiments, a molecular weight of 390,000 for $C1r_2C1s_2$ was found. The matchpoint was determined to be 43% ^2H_2O. Both results are consistent with composition data. The partial specific volume is 0.751 ml/mg. The radius of gyration at infinite contrast was found to be 17 nm for $C1r_2C1s_2$ and 1.1 nm for the cross section. Models for $C1r_2C1s_2$ were computed by the method of hard spheres, in which $C1r_2C1s_2$ was represented by spheres 0.87 nm diameter arranged in a straight rod of length 59 nm and a circular cross section of 3.2 nm. This rod can be bent at one or two places by up to 60° without significant effect on the calculated radii of gyration. The model is in agreement with published ultracentrifugation and electron microscopy data.**

The first component of complement (C1) is a macromolecular assembly of two distinct entities, C1q and $C1r_2C1s_2$. The binding of C1q to immune complexes causes conversion of the proenzymic $C1r_2C1s_2$ to the activated complex $C\bar{1}r_2C\bar{1}s_2$. On the basis of protease digestion and electron microscopic studies, the structure of C1q has been proposed to be most unusual—consisting of six globular heads attached to six collagenous stalks and resembling a bunch of tulips (1–5). The tetrameric complex $C1r_2C1s_2$ appears in the electron microscope to adopt an extended conformation, and ultracentrifugation data tend to support the proposal that the complex is extended in solution (6). Electron microscopy studies on the reconstituted chemically crosslinked C1 complex have been used to propose a tentative model in which $C1r_2C1s_2$ is wound within the stalks of the C1q molecule (7). Other biochemical data have been used to propose an alternative ring-like model (8).

Neutron scattering is a powerful low-resolution method for the study of macromolecule assemblies (9), particularly when used in conjunction with information available from other techniques such as electron microscopy. It has the added advantage that measurements are obtained from solution where it is known that the bound hydration shell of the glycoprotein does not affect interpretation.

Results of a preliminary characterization of C1q by using neutron scattering (10) substantially agreed with results from electron microscopy. Here we report on neutron studies of the $C1r_2C1s_2$ complex. The overall shape and cross-sectional dimensions of $C1r_2C1s_2$ indicate that this complex adopts an extended conformation in solution. The neutron data are considered together with a further analysis of ultracentrifugation experiments and allowed models of the $C1r_2C1s_2$ complex to be discussed.

The publication costs of this article were defrayed in part by page charge payment. This article must therefore be hereby marked "*advertisement*" in accordance with 18 U.S.C. §1734 solely to indicate this fact.

MATERIALS AND METHODS

Preparations of $C1r_2C1s_2$ and $C\bar{1}r_2C\bar{1}s_2$. Proenzymic C1r was purified from human serum by affinity chromatography as described (11). Proenzymic C1s and activated $C\bar{1}r$ and $C\bar{1}s$ were purified from human serum by using insoluble immune aggregates as described (12, 13). Each isolated protein was stored at 0°C in 5 mM triethanolamine·HCl/145 mM NaCl, pH 7.4. Proenzymic $C1r_2C1s_2$ and activated $C\bar{1}r_2C\bar{1}s_2$ complexes were prepared by mixing equimolar amounts of the appropriate subcomponents in the presence of 5 mM $CaCl_2$ and dialyzing against 10 mM Tris·HCl/150 mM NaCl/5 mM $CaCl_2$, pH 7.25. The amino acid and carbohydrate compositions are summarized in Table 1 (14–18).

The neutron experiments were performed in 10 mM Tris/150 mM NaCl/5 mM $CaCl_2$, pH 7.25, containing 75% or 100% ^2H_2O by volume. Dialysis was performed for 36 hr at 4°C in a specially constructed apparatus in which 0.4-ml samples could be dialyzed repetitively against 4 ml of buffer. This permitted extensive dialysis to equilibrium with minimal losses of sample and a relatively small volume of dialysis buffer. Concentrations of the $C1r_2C1s_2$ and $C\bar{1}r_2C\bar{1}s_2$ complexes in mg/ml were determined by using an extinction coefficient ($E^{280}_{0.1\%}$) of 1.06. The value 1.06 is the mean of the coefficients determined for proenzymic C1r and C1s (19). All neutron measurements were performed at 6 ± 0.5°C.

Neutron Scattering Measurements and Data Analysis. Data were measured on the neutron instrument D11 at the Institut-Laue-Langevin (20, 21). Data analysis followed conventional procedures (22). The forward scattering of neutrons extrapolated to zero momentum transfer, $I_{(0)}$, and the radius of gyration, R_G, were obtained from least squares fits by the Guinier relationship:

$$\ln I_{(Q)} = \ln I_{(0)} - R_G{}^2Q^2/3 \qquad [1]$$

in which $Q = 4\pi \sin \theta/\lambda$ (2θ is the scattering angle and λ is the wavelength). The corresponding cross-sectional parameters were obtained by using the relationship (23):

$$\ln I_{(Q)}\cdot Q = \ln I_{(Q)}\cdot Q - R_{XS}{}^2\, Q^2/2. \qquad [2]$$
$$(\lim Q \to 0)$$

Abbreviations: C1, first component of complement, composed of the distinct proteins C1q, C1r, and C1s; $C1r_2C1s_2$, calcium-dependent complex of C1 subcomponents C1r and C1s; overbar (as in $C\bar{1}r_2C\bar{1}s_2$), indicates the enzymatically active component.

§ Present address: Kennedy Institute, Bute Gardens, Hammersmith, London W6 7DW, United Kingdom.

Table 1. Amino acid and carbohydrate compositions (mol/mol of glycoprotein) of $C1r_2C1s_2$

	C1r*	C1s†
Nonpolar residues:		
Ala	33.3	40
Val	41.6	57
Leu	62.6	44
Ile	32.2	31
Phe	42.3	37
Tyr	37.2	35
Trp‡	11.9	10
Met	13.0	12
1/2 Cys	28.9	30
Pro	47.3	53
Total	350.3	349
Polar residues:		
Gly	69.7	71
Asp§	45.2	48
Glu§	57.8	50
Ser	44.6	51
Thr	40.6	35
Asn§	35.4	37
Gln§	37.5	33
Lys	41.3	42
Arg	44.3	30
His	21.4	14
Total	437.8	411
Protein matchpoint, % ^2H_2O¶	42.6	42.3
Carbohydrate residues‡:		
Man	7.5	5.9
Gal	9.2	5.6
GlcNAc	15.1	8.4
GalNAc	2.2	0.8
NeuNAc	5.2	7.5
Total	39.2	28.2
Carbohydrate matchpoint, % ^2H_2O¶	46.9	48.8
Carbohydrate, % (wt/wt) of total glycoprotein	8.1	6.8

*From ref. 17.
†Unpublished data.
‡From ref. 18.
§Approximated by reference to Dayhoff (14).
¶Residue volumes were taken from refs. 15 and 16. The nonexchange of the main-chain exchangeable protons was taken to be 10%.

A detector–sample distance of 10.66 m, a collimation of 10 m, and λ of 1.20 nm were used for the R_G measurements; for the R_{XS} measurements the values were 2.66 m, 2.5 m, and 0.80 nm, respectively. Spectra were referenced on an absolute scale on the basis of the incoherent scattering of neutrons from a 1-mm water sample. Backgrounds were measured by using an empty cell and a cadmium sample.

The R_G and R_{XS} values were analyzed according to the Stuhrmann equation (24). For a distribution of scattering densities within a macromolecule that is concentric on average, a simplified form of the Stuhrmann equation may be used:

$$R_G^2 = R_C^2 + \alpha\Delta\rho^{-1} \quad [3]$$

in which $\Delta\rho$ is the contrast difference between the macromolecule and the solvent, R_C is the radius of gyration at infinite contrast, and α is related to the radial fluctuation of scattering densities within the macromolecule (9). Knowledge of the R_C values leads to the determination of the length L of the straight rod-like particle (25):

$$L^2 = 12\,(R_{C-G}^2 - R_{C-XS}^2). \quad [4]$$

The value of $I_{(0)}$/concentration (c) measured in H_2O and normalized on the basis of the incoherent scattering of H_2O leads to the molecular weight M_r (26). In application to $C1r_2C1s_2$ at a wavelength of 1.20 nm, the composition in Table 1 was used to derive the following expression:

$$M_r = 18.2 \times 10^5 \times I_{(0)}/c. \quad [5]$$

For the cross-sectional $I_{(Q)}\cdot Q/c$ (lim $Q\to 0$) measured with a wavelength of 8.00 nm, the M_r per unit length M_r/L nm^{-1} is given by (26):

$$M_r/L = 4.86 \times 10^6 \times I_{(Q)}\cdot Q/c \text{ (lim } Q\to 0). \quad [6]$$

For modeling calculations, the method of hard spheres was used in order to calculate R_C and the full scattering curve. Assemblies of spheres were generated, and these were used for the Debye calculation of the scattering curve which in turn was used to calculate R_G and R_{XS} values. The ranges of Q over which calculation of R_G and R_{XS} values from the scattering curve is allowed were determined from the calculated scattering curves. These simulations were used to predict the dependence of $I_{(0)}$ and R_G on the Q range used for analysis of the neutron data. For the present experiments, fitting of the Guinier plots in the $Q\cdot R_G$ range of 0.2–1.0 and $Q\cdot R_{XS}$ range of 0.5–1.6 satisfy Eqs. 1 and 2 to within a few percent on the basis of model A in Fig. 4. The curvature of the Guinier plots shown in Fig. 1 could also be taken into account in determining R_G.

Interpretation of Frictional Coefficients. Combination of the Stokes–Einstein equation for diffusion (27) and the Svedberg equation for ultracentrifugation (28) gives the following general expression:

$$s^0_{20,w} = \frac{M_r\,(1 - \bar{v}\rho)}{N_a\langle f\rangle} \quad [7]$$

in which $s^0_{20,w}$ is the sedimentation coefficient, M_r is the molecular weight, $\bar{v}$ is the partial specific volume, ρ is the solvent density, N_a is Avogadro's number, and $\langle f\rangle$ is the frictional coefficient. For a sphere, $\langle f\rangle$ is given by $6\pi\eta a$ in which η is the solvent viscosity and a is the Stokes radius. There is no exact theory for the hydrodynamic properties of circular cylindrical rods, unlike the case of ellipsoidal objects (29). However, several approximate expressions for the frictional coefficients of straight cylinders have been proposed, which show reasonable but not perfect agreement with experiments (29).

(*i*) In a previous analysis (6) of $C1r_2C1s_2$, a hydrodynamic model was derived from ref. 30, which was based on the 1960 theory of Broersma (31). In Eq. 7 above, the frictional coefficient $\langle f\rangle$ is replaced by $6\pi\eta L/[2\ln(2L/d) - 0.2316 + d/L]$ in which L is the length of the rod and d is its diameter.

(*ii*) An updated expression of Broersma (31) given by this author was used in ref. 32, where the frictional coefficient was described by $6\pi\eta L/[2\delta - (\gamma_\parallel + \gamma_\perp)]$ in which $\delta = \ln 2L/d$ and L and d are as above. The values of $\gamma_\parallel$ and $\gamma_\perp$ are given by:

$$\gamma_\parallel = 1.27 - 7.4\,(\delta^{-1} - 0.34)^2$$

$$\gamma_\perp = 0.19 - 4.2\,(\delta^{-1} - 0.39)^2. \quad [8]$$

(*iii*) In refs. 29 and 33, a type of expression similar to ii is given (which these authors hold fits more closely to the available theoretical and experimental data) in which the frictional coefficient is described by $3\pi\eta L/[\ln p + (\gamma_\parallel + \gamma_\perp)/2]$ and $p = L/d$ with L and d as above and $\gamma_\parallel$ and $\gamma_\perp$ are given by:

$$\gamma_\parallel = -0.207 + 0.980\,p^{-1} - 0.133\,p^{-2}$$

$$\gamma_\perp = 0.839 + 0.185\,p^{-1} - 0.233\,p^{-2}. \quad [9]$$

RESULTS AND DISCUSSION

Analysis of the scattering curve of $C1r_2C1s_2$ is shown in Fig. 1 for the sections corresponding to the Guinier region and the cross-sectional region. Plots of ln I at low Q^2 and ln $I{\cdot}Q$ against Q^2 were linear. From the H_2O measurement of $I_{(0)}/c$, a molecular weight of 390,000 ± 40,000 was calculated. This is in good agreement with apparent values of 336,000–364,000 measured from $NaDodSO_4$/polyacrylamide gel electrophoresis of the a and b chains from the isolated fragments (18). The data of Table 1 suggest a value of 380,000 and this is used below. Although the counting statistics were poor in this H_2O measurement, the cross-sectional measurements of $I_{(Q)}{\cdot}Q/c$ lead to a molecular weight per unit length of 5,000 ± 1,000/nm. The full-contrast variation experiment depicted in Fig. 2 showed that $C1r_2C1s_2$ has a matchpoint of 43% ^2H_2O. This can be compared with a matchpoint (i.e., scattering density) of 43% ^2H_2O (Table 2) calculated from the composition data. The mass density of $C1r_2C1s_2$ corresponds to $\bar{v}$ = 0.751 ml/g (Table 2). These considerations indicate that the neutron scattering properties of $C1r_2C1s_2$ in solution are accounted for in terms of its known composition and that $C1r_2C1s_2$ has an elongated shape in solution.

The analyses of the radii of gyration are summarized in Fig. 3. Within the error of measurements, the Stuhrmann plot of the R_G values is linear, and the value of R_{C-G}, the radius of gyration at infinite contrast, was determined to be 17 ± 2 nm. That for R_{C-XS} was estimated as 1.1 ± 0.1 nm. From these values, the length of the straight rod is 59 ± 6 nm, and hence M_r/L is determined to be 6,400 ± 1,000/nm in agreement with the above value. By comparison, the value of R_{C-G} for a globular protein of M_r 380,000 is calculated to be 4 nm. The slope α was determined to be about 20×10^{-3}. If the value of α measured for small globular proteins is rescaled on the basis of its proportionality to R_C^2, α for $C1r_2C1s_2$ is predicted to be about 6×10^{-3}. $C1r_2C1s_2$ thus possesses a surface of hydrophilic amino acid (and carbohydrate) residues and a core of hydrophobic residues.

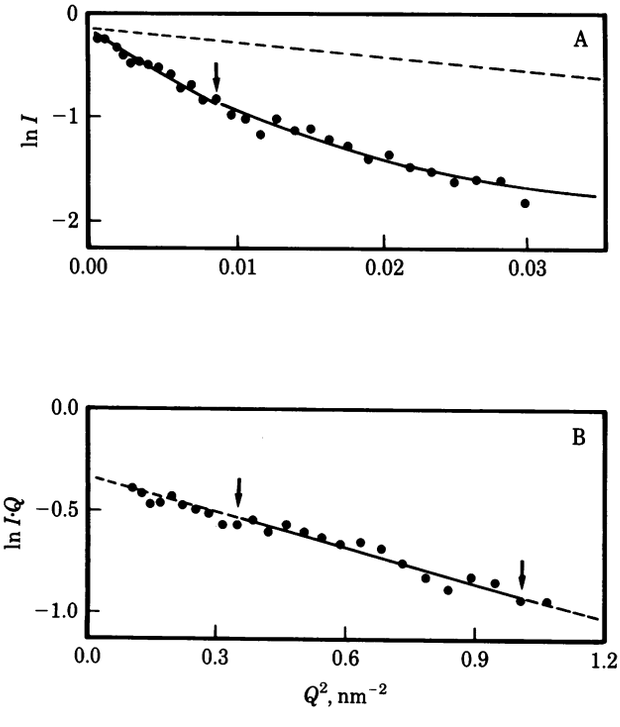

FIG. 1. Scattering curves of $C1r_2C1s_2$ in 100% ^2H_2O buffers in a concentration of 1.10 mg/ml. (*A*) Guinier plot of ln I vs. Q^2. The arrow corresponds to $Q{\cdot}R_G$ = 1.4. The solid line at $Q^2 > 0.01$ nm^{-2} corresponds to the calculated Debye scattering curve. The dotted line corresponds to R_G = 4 nm, which would be expected if $C1r_2C1s_2$ had a globular shape. (*B*) Cross-sectional plot of ln $I{\cdot}Q$ vs. Q^2; the range $0.6 < Q{\cdot}R_{XS} < 1.1$ is marked by arrows.

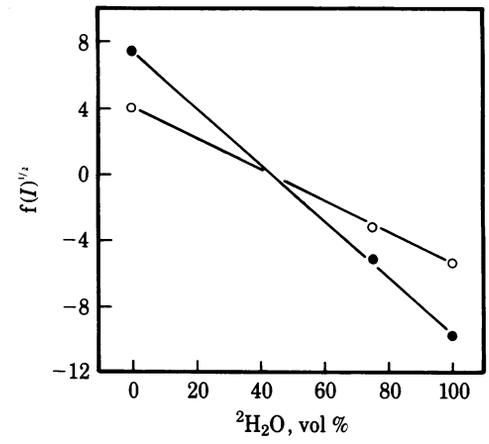

FIG. 2. Determination of the matchpoint of $C1r_2C1s_2$ from a plot of $\sqrt{I_{(0)}/ctT_s}$ and $\sqrt{I_{(Q)}{\cdot}Q/ctT_s}$ vs. concentration of ^2H_2O; T_s is the sample transmission, c is the concentration, and t is the sample thickness. ●, Guinier plots; ○, cross-sectional plot. Sample concentrations ranged between 1.1 and 1.3 mg/ml.

Models for the shape of $C1r_2C1s_2$ were developed on the basis of a Debye calculation of an array of hard spheres (Fig. 4; Table 3). The physical volume of $C1r_2C1s_2$ of 474 nm^3 (which for these calculations was expressed in terms of the volume of the same number of equivalent cubes) and the total and cross-sectional values of the R_G from the Stuhrmann plots were used as constraints. That the R_G of the neutron shape is less than the R_G of the physical shape because of ^1H–^2H exchange in $C1r_2C1s_2$ is not considered in the simulations; the errors are <1% (unpublished calculations). A straight rod of 168 spheres corresponding to cubes of side 1.4 nm with total length 59 nm and square cross section of 4 spheres satisfied the R_G and R_{XS} parameters. These simulations were improved with the use of 1,344 spheres of diameter 0.87 nm, and these led to the final values of Table 3. The application of smearing corrections with a Gaussian function has little influence on the R_G values. Because $C1r_2C1s_2$ is a tetrameric association of C1r and C1s, further calculations were made in which the rod was bent in one or two positions in order to examine the effects of segmental flexibility. A family of solutions exists in which segmental movements of up to 60° can occur which leaves R_G and R_{XS} smaller by up to only 8%. Further conformational changes have larger effects on R_G and therefore can be ruled out. Some or all of the structures of this family could coexist in equilibrium with one another. Furthermore, a small amount (<20%) of ring-like shapes (8) cannot be excluded. In such cases the dimensions reported here would represent a population-weighted average. In this context, large R_G values are favored in the experimentally determined value in a group of particles of identical mass but different shapes (34).

Table 2. Characteristics of total $C1r_2C1s_2$

Total $C1r_2C1s_2$	Calculated	Experimental
Matchpoint, % ^2H_2O*	42.8	43
Volume, nm^3*	474	
Molecular weight × 10^{-3}	375	390
$\bar{v}$, ml/g	0.751	
$\Sigma b/M$ in H_2O, cm × 10^{-12}	0.02357	

* See footnote ¶ in Table 1.

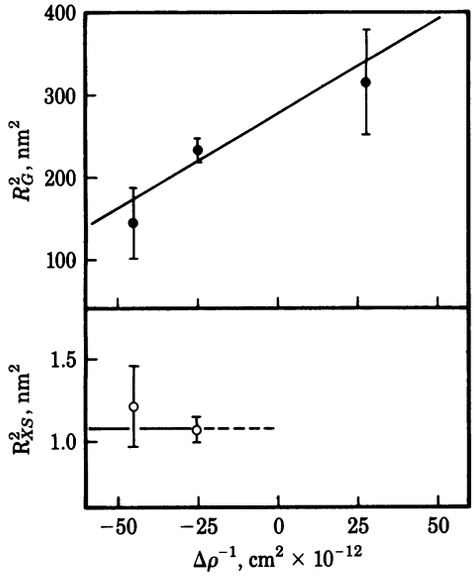

FIG. 3. Stuhrmann plots of R_G^2 (●) and R_{XS}^2 (○) versus $\Delta\rho^{-1}$.

This model of a rod of length 59 nm and circular cross section 3.2 nm is compared with the hydrodynamic properties of the $C1r_2C1s_2$ complex determined from ultracentrifugation experiments. Data on the shape of $C1r_2C1s_2$ published by Tschopp *et al.* (6) suggest elongated particles of length 51 ± 2 nm from electron microscopy and of length 64 ± 4 nm and diameter 3.4 ± 0.1 nm from ultracentrifugation. From electron microscopy, Strang *et al.* (7) proposed an elongated particle of approximate length 59 nm. The R_G of straight cylindrical objects with these dimensions are 14.8 ± 0.6 nm, 18.5 ± 1.1 nm, and 17.1 nm.

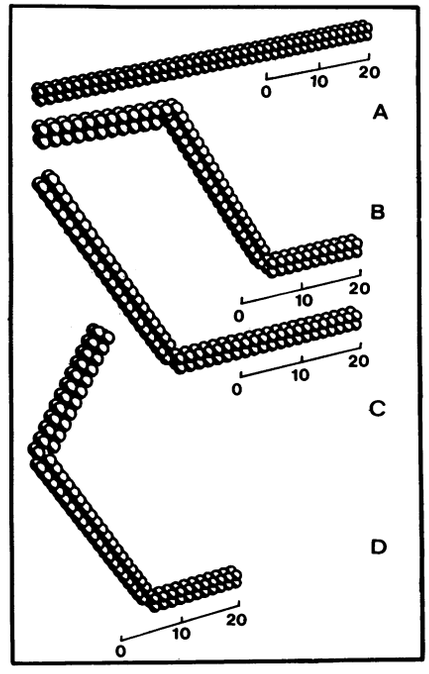

FIG. 4. Selection of possible perspective rod-like models of $C1r_2C1s_2$ represented by 168 spheres corresponding to the cubic array that was used in the Debye simulations of the scattering curves. The four models lead to similar R_G and R_{XS} values (Table 3); all bends are 60° in magnitude. Each sphere is 1.4 nm in diameter. The size of each model is indicated by the scale in increments of 10 nm. The models depicted are only a selection of those consistent with neutron scattering data; the presence of small amounts of ring-like forms is not excluded.

Table 3. Shape parameters for $C1r_2C1s_2$ by experiment and modeling*

Model calculations†	R_G, nm	R_{XS}, nm
	17.0	
Straight rod		1.1‡
Two bends of ±60°§	15.6	1.1
One bend of 60°	16.1	1.1
Two bends of 60°	15.6	1.1

* Experimental (unactivated $C1r_2C1s_2$): R_{C-G} = 17 ± 2 nm; R_{C-XS} = 1.1 ± 0.1 nm.

† The 1,344 spheres are of diameter 0.87 nm set in a cubic array of 84 × 4 × 4 (Fig. 4); the radius of the sphere corresponds to the volume of each cube.

‡ R_{XS} is 1.1 nm if a uniform cylindrical rod of diameter 3.2 nm is assumed (ref. 25; Table 4).

§ The values of R_G are 17.0 and 13.5 nm for bends of ±30° and ±90°, respectively.

These are consistent within error with the R_C determined by neutron scattering (Table 3) of 17 ± 2 nm.

To make some choice in this range of dimensions, we used hydrodynamic theory *iii* (see *Materials and Methods*) as a filter, although Table 4 shows calculations for all three of the theories because of their previous application to this system. The use of theory *iii* is dictated by Garcia de la Torre and Bloomfield's comments (p. 110 of ref. 30). With the improved value for $\bar{v}$ (see above), the experimental value of $s^0_{20,w}$ of 8.7 S can be satisfactorily accounted for, once allowance is made for flexibility in the rod (29) and a degree of hydration of 0.3 (35). If the rod is allowed to bend with or without being flexible, the discussion in ref. 30 shows that the viscosity η becomes smaller but that the translational diffusion coefficient D_T remains unchanged, implying that the $s^0_{20,w}$ value will increase. This means that an increase in the physical length of the rod is required to maintain the experimental value of $s^0_{20,w}$ = 8.7 S once the rod is allowed to bend by much more than 60°.

The model with the shortest length leads to $s^0_{20,w}$ values that are too large (Table 4), and flexibility would increase these values still further. The longest rod, length 64 nm, leads to quite close agreement with $s^0_{20,w}$ but its R_G value is at the limit of our determination. The intermediate value derived by ourselves and Strang *et al.* (7) is the most consistent with the experimental data. The joint findings from neutron scattering, ultracentrifugation, and electron microscopy (7) therefore show that the $C1r_2C1s_2$ complex has an extended rod-like shape of length 59 ± 6 nm and diameter 3.2 nm. The solution data do not distin-

Table 4. Calculations of the hydrodynamic properties of $C1r_2C1s_2$

	Theoretical sedimentation coefficient, S*		
$L{\cdot}d$, nm	Model *i*	Model *ii*	Model *iii*
Unhydrated straight rod models:			
51 × 3.4 (6)	10.8	8.8	10.0
59 × 3.2 (7; this study)	9.9	8.2	9.2
64 × 3.1 (6)†	9.4	7.9	8.7
Hydrated straight rod models:			
51 × 4.0 (6)	10.2	8.1	9.4
59 × 3.8 (7; this study)	9.4	7.7	8.7
64 × 3.6 (6)	9.0	7.5	8.4

* Experimental value (6.35): 8.7 S. Calculations are based on M_r = 380,000, $\bar{v}$ = 0.751 ml/g, ρ = 0.9982 g/ml, and η = 0.01002 poise. The value of d is derived from the volume of the rod and its length.

† A diameter of 3.4 nm was derived in ref. 6; the calculation of $s^0_{20,w}$ is almost unaffected.

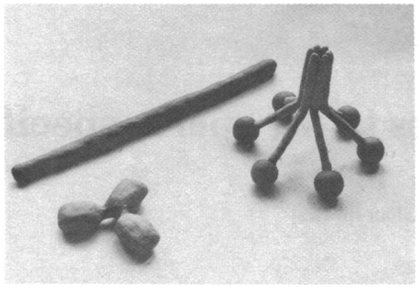

FIG. 5. Plasticene scale models of IgG, C1q, and $C1r_2C1s_2$. The dimensions are from refs. 38 and 39 for IgG, from refs. 2 and 11 for C1q, and from this work for $C1r_2C1s_2$. The $C1r_2C1s_2$ complex is shown as a straight rod, although this rod may be bent (Fig. 4).

guish between straight rods or rods with up to 60° of bend. Preliminary data were acquired for activated $\overline{C1r}_2\overline{C1s}_2$ in 100% ^2H_2O; these suggest the same elongated dimensions but again do not discriminate among the models shown in Fig. 4. Therefore, there is no clear evidence in the neutron scattering data for any major conformational change leading to large changes in dimensions in the activation of $C1r_2C1s_2$, at least in the absence of C1q. In this context, we note the similar $s^0_{20,w}$ of 8.7 S observed for the activated species (36). However, some changes must occur, reflecting the cleavage of covalent bonds. In this regard, it previously was shown that the number of calcium-binding sites changes upon activation (37).

Finally, we show in Fig. 5 a comparison of the relative dimensions of IgG, C1q, and the straight rod representation of $C1r_2C1s_2$.

We thank the Institut-Laue-Langevin for the neutron facilities and Dr. R. P. May for useful discussions, the European Molecular Biology Laboratory for the use of biochemical facilities, and Professor M. G. Colomb for useful discussions. We gratefully acknowledge financial support from the Medical Research Council, the Science and Engineering Research Council, and the European Molecular Biology Laboratory.

1. Porter, R. R. & Reid, K. B. M. (1979) *Adv. Protein Chem.* **33,** 1–71.
2. Reid, K. B. M. & Porter, R. R. (1981) *Annu. Rev. Biochem.* **50,** 433–464.
3. Shelton, E., Yonemasu, K. & Stroud, R. M. (1972) *Proc. Natl. Acad. Sci. USA* **69,** 65–68.
4. Knobel, R., Villiger, W. & Isliker, H. (1975) *Eur. J. Immunol.* **5,** 78–82.
5. Brodsky-Doyle, B., Leonard, K. R. & Reid, K. B. M. (1976) *Biochem. J.* **159,** 279–286.
6. Tschopp, J., Villiger, W., Fuchs, H., Kilchherr, E. & Engel, J. (1980) *Proc. Natl. Acad. Sci. USA* **77,** 7014–7018.
7. Strang, C. J., Siegel, R. C., Phillips, M. L., Poon, P. H. & Schumaker, V. N. (1982) *Proc. Natl. Acad. Sci. USA* **79,** 586–590.
8. Colomb, M. G., Bensa, J. C., Villiers, C. L. & Arlaud, G. J. (1982) *Ann. Immunol. Inst. Pasteur (Paris)* **133C,** 155–164.
9. Koch, M. H. J. & Stuhrmann, H. B. (1979) *Methods Enzymol.* **59,** 670–706.
10. Gilmour, S., Randall, J. T., Willan, K. J., Dwek, R. A. & Torbet, J. (1980) *Nature (London)* **285,** 512–514.
11. Villiers, C. L., Duplaa, A.-M., Arlaud, G. J. & Colomb, M. G. (1982) *Biochim. Biophys. Acta* **700,** 118–126.
12. Arlaud, G. J., Villiers, C. L., Chesne, S. & Colomb, M. G. (1980) *Biochim. Biophys. Acta* **616,** 116–129.
13. Arlaud, G. J., Sim, R. B., Duplaa, A.-M. & Colomb, M. G. (1979) *Mol. Immunol.* **16,** 445–450.
14. Dayhoff, M. O. (1978) *Atlas of Protein Sequence and Structure* **5,** 36–36.
15. Clothia, C. (1975) *Nature (London)* **254,** 304–308.
16. Perkins, S. J., Miller, A., Hardingham, T. E. & Muir, H. (1981) *J. Mol. Biol.* **150,** 69–95.
17. Arlaud, G. J., Gagnon, J. & Porter, R. R. (1982) *Biochem. J.* **201,** 49–59.
18. Sim, R. B. (1981) *Methods Enzymol.* **80,** 26–42.
19. Sim, R. B., Porter, R. R., Reid, K. B. M. & Gigli, I. (1977) *Biochem. J.* **163,** 219–227.
20. Ibel, K. (1976) *J. Appl. Crystallogr.* **9,** 269–309.
21. Timmins, P. A. & May, R. P. (1981) *I.L.L. Internal Publication 81TI53S.*
22. Ghosh, R. (1978) *I.L.L. Internal Publication 78GH247T.*
23. Luzzati, V. (1960) *Acta Crystallogr.* **13,** 939–945.
24. Ibel, K. & Stuhrmann, H. B. (1975) *J. Mol. Biol.* **93,** 255–266.
25. Pilz, I. (1973) in *Physical Principles and Techniques of Protein Chemistry, Part C,* ed. Leach, S. J. (Academic, New York).
26. Jacrot, B. & Zaccai, G. (1981) *Biopolymers* **20,** 2413–2426.
27. Berne, B. J. & Pecora, R. (1976) *Dynamics Light Scattering* (Wiley, New York), pp. 143–146.
28. Van Holde, K. E. (1971) *Physical Biochemistry,* (Prentice-Hall, Englewood Cliffs, NJ).
29. Garcia de la Torre, J. & Bloomfield, V. A. (1981) *Q. Rev. Biophys.* **14,** 81–139.
30. Bloomfield, V., Dalton, W. O. & Van Holde, K. E. (1967) *Biopolymers* **5,** 135–159.
31. Broersma, S. (1960) *J. Chem. Phys.* **32,** 1626–1631; 1632–1635.
32. Newman, J., Swinney, H. L. & Day, L. A. (1977) *J. Mol. Biol.* **116,** 593–606.
33. Tirado, M. M. & Garcia de la Torre, J. (1979) *J. Chem. Phys.* **71,** 2581–2588.
34. Guinier, A. & Fournet, G. (1955) *Small Angle Scattering of X-Rays* (Wiley, New York), pp. 149–151.
35. Tanford, C. (1961) *Physical Chemistry of Macromolecules* (Wiley, New York), p. 359.
36. Arlaud, G. J., Chesne, S., Villiers, C. L. & Colomb, M. G. (1980) *Biochim. Biophys. Acta* **616,** 105–115.
37. Villiers, C. L., Arlaud, G. J., Painter, R. H. & Colomb, M. G. (1980) *FEBS Lett.* **117,** 289–294.
38. Amzel, L. M. & Poljak, R. J. (1979) *Annu. Rev. Biochem.* **48,** 951–997.
39. Huber, R., Deisenhofer, J., Colman, P. M., Matsushima, M. & Palm, W. (1976) *Nature (London)* **264,** 415–420.